3rd Biennial International Conference on Powertrain Modelling and Control (PMC 2016)
Testing, Mapping and Calibration
7th-9th September 2016, Loughborough University, UK

Elastodynamics of Piston Compression Rings

R. Turnbull[1*], S.R. Bewsher[1], M. Mohammadpour[1], R. Rahmani[1], H. Rahnejat[1], G. Offner[2]

[1] Wolfson School of Mechanical, Electrical and Manufacturing Engineering, Loughborough University, UK

[2] AVL List GmbH, Graz, Austria

[*] Corresponding author: R.Turnbull@lboro.ac.uk

Abstract

The piston ring pack accounts for a disproportionate amount of the total engine frictional losses. The frictional behaviour of piston rings is significantly affected and governed by its flexible dynamics. The dynamically changing shape of the ring determines its contact geometry with the cylinder liner and hence affects the frictional losses. The compression ring undergoes a multitude of complex motions during the engine cycle prescribed by the gas pressure, contact reaction, ring tension, friction between the ring and its groove and inertial forces that excite a plethora of the ring's modal responses. This adversely compromises the functionality of the ring through a number of undesired phenomena such as ring flutter, twist, rotation and jump. Therefore, a prerequisite for improving the prediction of tribological conditions is an accurate determination of the ring's elastodynamic response. This paper presents a methodology to directly solve the governing differential equations of motion for different forms of beam cross-section, where the shear and mass centres are not coincident, typical of the complex cross-sections of a variety of different piston compression rings. Combined numerical and experimental investigations are undertaken to determine the dynamic behaviour of the compression ring.

Keywords: *Compression Ring, Elastodynamics, Incomplete ring, Coupled bending- torsion*

1-Introduction

Increasingly stringent legislation and directives set emission targets for vehicle manufactures. Furthermore, fuel efficiency has progressively become a key commercial attribute. Another key driver in powertrain developments is the customer expectation for increased output power. These seemingly contradictory demands point to the common attributes of reduced powertrain losses and light weight and compact constructions. Performance improvements in fuel economy, power output and emissions have to be realised at minimal cost per vehicle.

The piston ring pack accounts for a disproportionate amount of the total engine losses (up to 25% of the parasitic losses, with the compression ring alone accounting for approximately 5% of the total engine losses) [1]. This provides the motivation behind this investigation. The frictional

behaviour of piston rings is significantly affected by their elastodynamic behaviour (flexible modal dynamics) [2, 3]. The dynamically changing ring shape alters the contact geometry and hence the resulting frictional losses. Therefore, a combined dynamics and tribological study of the problem is required, termed as tribo-dynamics.

The primary function of the compression ring is to act as a seal between the piston ring pack and the combustion chamber to reduce power loss and blow-by. To ensure an effective seal, good conformity between the ring and cylinder liner is essential. A delicate balance between good conformability and excessive friction, heat generation and wear within the contact is critical for effective operation. Furthermore, it is essential that the compression ring transfers the surplus heat away from the piston to the cylinder wall. Realising the above fundamental requirements ensures effective engine performance.

The compression ring undergoes a multitude of complex motions during the engine cycle, prescribed by the applied gas pressure, contact reaction, ring tension, friction between the ring and groove and the inertial forces that excite a plethora of the ring's modal responses. These adversely compromise the functionality of the ring through a number of undesired phenomena such as ring flutter, twist, rotation and jump [2-4].

The dynamic behaviour of the compression ring is a prerequisite for improving its tribological performance with the cylinder liner conjunction during the engine cycle, which constitutes the focus of the current investigation. The transient nature of the contact conditions provides an insight into the mechanisms contributing to frictional losses, thus engine efficiency. The applied conditions; ring loading and piston kinematics, as well as ring geometry and topography and bore shape are key parameters for the tribological study of the conjunction which require prediction of generated contact pressures, film thickness, thus the determination of load carrying capacity and friction and errant dynamics' power losses [5-10].

An analytical solution for in-plane motions of a thin circular ring is presented by Lang [11] and for out-of-plane motions by Ojalvo [12]. These equations of motion consider the in-plane and out-of-plane motions as uncoupled. The solution to the in-plane dynamics is utilised for the evaluation of ring friction [2, 13] by solving the equations of motion detailed in [11]. The investigation was expanded to the detailed effect of compression ring dynamics on friction and power loss within the internal combustion engines [14], utilising the out-of-plane solution provided in [12]. The solution considered four degrees of freedom and required the cross section to be modelled as an equivalent rectangle.

A curved beam solution is provided for a uniform curve bar [15]. Straight beam element models have been presented to approximate the geometry of the piston ring [16]. The model utilises Timoshenko beam theory and assumes that the shear centre and the mass centre of the cross-section are coincident. The dynamic stiffness matrix method has been utilised to approximate a solution for the elastodyamics of crankshaft systems [17]. The dynamic stiffness matrix of the individual piston ring beam elements can be concatenated as detailed by [18] to construct the overall dynamic stiffness matrix of the piston ring system. The dynamic stiffness matrix method

embeds and solves the mass and stiffness terms in a frequency-dependent matrix, where the terms are all functions of the natural frequency of the system. The solution is derived from Eulerian beam theory and assumes that the shear centre and mass centre of the cross section are coincident. Coupled solutions to evaluate different forms of complex cross sectioned beam elements have been reported, including by Rao and Carnegie [19] who showed that mode coupling resulted in a significant influence on the frequency response of the system.

This paper presents a methodology to directly solve the governing differential equations of motion for a beam section. In particular, the method accounts for different forms of beam cross sections, where the shear and mass centres are not coincident, typical of the complex cross sections of a variety of different piston compression rings.

2-Numerical Model

2.1-Direct Integration Method

A numerical model is created to model the elastodynamics of the piston compression ring. Euler's beam theory is utilized for the modelling of the ring behaviour in bending in its *xz* and *xy* principal planes, as well as in torsion and axial extension-compression (Figure 1).

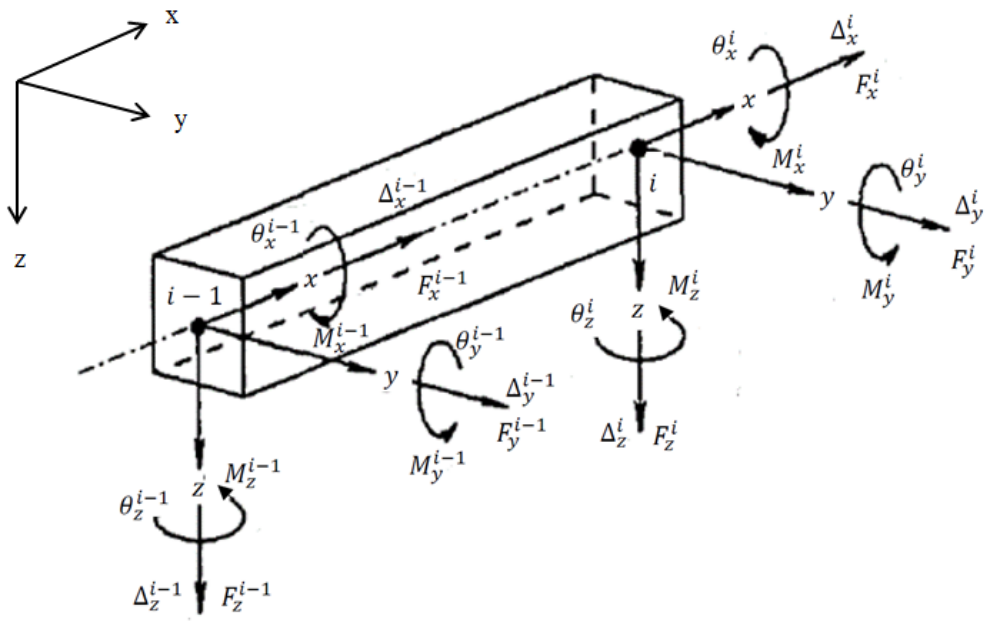

Figure 1: The beam element with according coordinate system

The governing differential equations for the beam are discretised and directly solved using a central difference finite difference explicit discretisation method. The solution for the ring elastic deformation under applied loads is found by performing direct integration in the time domain.

All the important degrees of freedom are considered in the current investigation [20]. The Euler beam model includes the coupled torsion-bending equations of motion [19]. This coupling occurs for beam sections with non-coincident mass and shear centres, typical of the complex cross sections of the piston rings (Figure 1). Different forms of cross section are considered by the coupling arms y_α and z_α acting along the y and z axes respectively. The values of y_α and z_α are obtained by determining the co-ordinate distance between the centre of shear and the centre of mass of the beam cross section. Thus:

$$EJ_{yy}\frac{\partial^4 \Delta z}{\partial x^4} + \rho A\frac{\partial^2 \Delta z}{\partial t^2} - \rho A y_\alpha \frac{\partial^2 \theta_x}{\partial t^2} = 0 \quad (1)$$

$$EJ_{zz}\frac{\partial^4 \Delta y}{\partial x^4} + \rho A\frac{\partial^2 \Delta y}{\partial t^2} + \rho A z_\alpha \frac{\partial^2 \theta_x}{\partial t^2} = 0 \quad (2)$$

$$GJ_p\frac{\partial^2 \theta_x}{\partial x^2} - \rho J_p\frac{\partial^2 \theta_x}{\partial t^2} + \rho A y_\alpha \frac{\partial^2 \Delta z}{\partial t^2} - \rho A z_\alpha \frac{\partial^2 \Delta y}{\partial t^2} = 0 \quad (3)$$

$$\rho A\frac{\partial^2 \Delta_x}{\partial t^2} - EA\frac{\partial^2 \Delta_x}{\partial x^2} = 0 \quad (4)$$

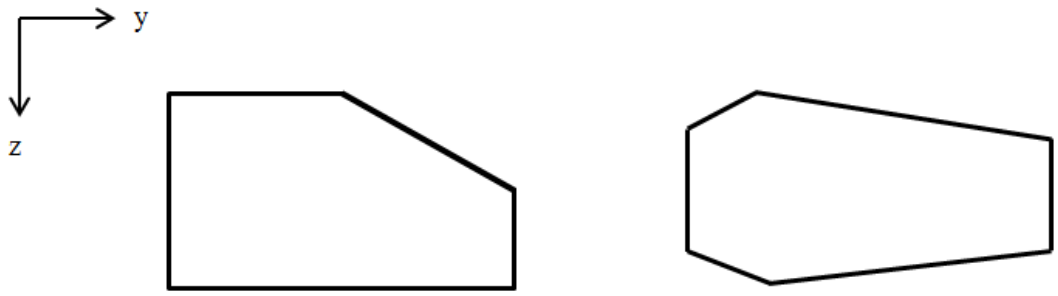

Figure 2: Piston ring cross sections

The system of differential equations (1)–(4) are transformed from the Cartesian frame of reference into cylindrical coordinates, where the equations of motion of the compression ring are best represented. Figure 2 is a schematic representation of the ring cross sections. In order to examine the accuracy of the model in the frequency domain, the mid-point of the beam is subjected to kinematic excitation (Figure 3). In the integrated tribo-dynamic model, all applied forces need to be considered. The material and geometrical properties of the piston ring are provided in Table 1.

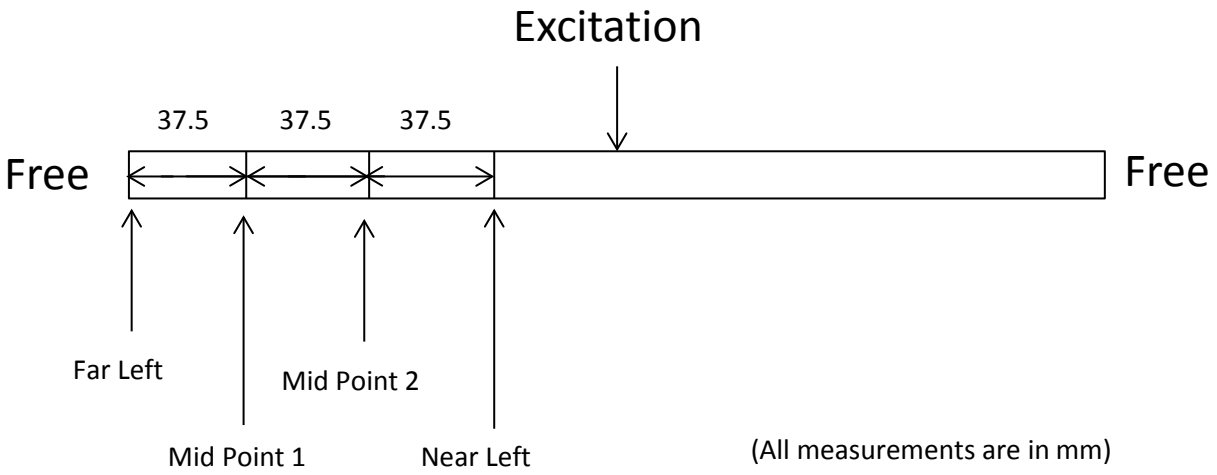

Figure 3: Schematic of the numerical model

Table 1: Compression ring properties

Elastic modulus (E)	203 GPa
Shear modulus (G)	78.7 GPa
Material density (ρ)	7850 kg/m^3
Poisson ratio (v)	0.3
Ring thickness (b)	1.15 x 10^{-3} m
Ring height (h)	3.5 x 10^{-3} m
Ring length (L)	300 x 10^{-3} m
Cross-sectional area (A)	4.06 x 10^{-6} m^2
Second area moment of inertia (Jyy)	4.436 x 10^{-13} m^4
Second area moment of inertia (Jzz)	4.109 x 10^{-12} m^4
Polar area moment of inertia (Jp)	4.552 x 10^{-12} m^4

Excitation is prescribed as a function of displacement (x_f) and velocity (v_f):

$$x_f = M2\pi f \cos(2\pi f t) \tag{5}$$

$$v_f = -M4\pi^2 f^2 \sin(2\pi f t) \tag{6}$$

where, M is the amplitude of oscillation (m), f is the applied vibration frequency (Hz) and t is time (s).

2.2-Finite Element Analysis

In order to evaluate the accuracy of the model in the frequency domain, a frequency-amplitude sweep is performed. The predictions of the frequency response calculated for the ring dynamics are compared with those from a finite element model (FEM), as well as with experimental results carried out under the same conditions. The FEM comprises tetrahedral elements with 2,100 nodes, each with 6 degrees of freedom. The results are obtained in PATRAN/NASTRAN for free-free boundary conditions applied to the ring ends. The material and geometric properties utilized in the finite element analysis are those listed in Table 1.

3-Experimental Measurements

Figure 4 shows the experimental rig with appropriate in-situ constraints, comprising a shaker, shaker extension, a force transducer, clamp and a piston compression ring. The clamp is threaded directly onto the force transducer which in turn is threaded directly onto the shaker extension and thus the shaker itself. This ensures a secure system configuration between the shaker and the clamp. The piston compression ring is rigidly mounted onto the clamp by tightening the screw set. The contact area between the clamp and the ring is minimised, utilising the configuration detailed in Figure 4. The piston ring is positioned both upright and laterally for out-of-plane and in-plane vibrations respectively. This is to mitigate the effect of gravity.

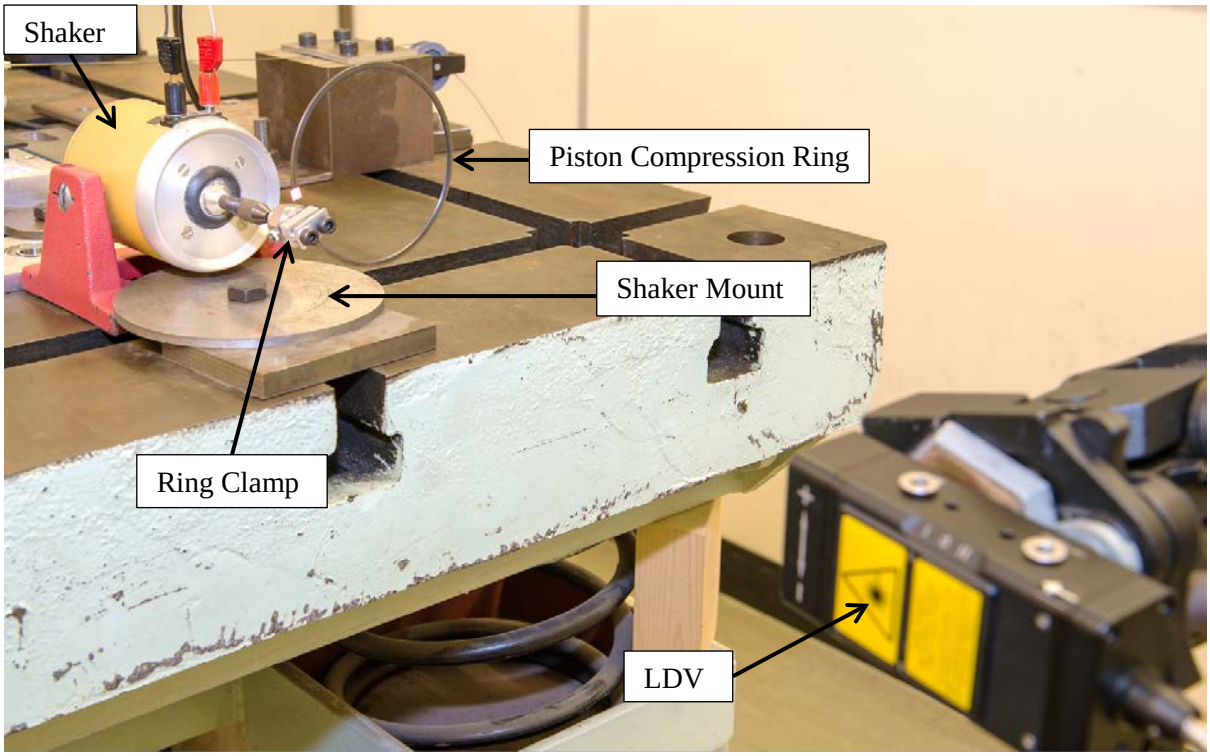

Figure 4: Experimental setup

A Laser Doppler vibrometer (LDV) is positioned appropriately in order to measure the vibrations of the compression ring as the elastic wave runs through its structure. The LDVs measure the velocity of the lateral oscillations of the piston ring through a Doppler shift in the frequency of light, scattered by a moving object [21]. Nyquist criterion specifies that a sampling rate of at least twice the highest expected response frequency should be used. Baker et al [2] noted that the first three modal responses were observed during the engine cycle, with the inclusion of the first seven modes not altering the results. Therefore, as a benchmark, the first seven modes of the ring up to a frequency of 6000 Hz are required in the current investigation. In order to capture the frequency range of interest a conservative sampling rate of 32,000 is utilised. A list of instrumentation utilised in the experimental investigation is provided in Table 2.

Table 2: List of instrumentation

Apparatus	Transducer Sensitivity	Amplifier Setup Sensitivity
Vibrometer (lateral Displacement)	200 µm/V	0.02 mm/V
Force Transducer	3.96 pC/N	1 V/N

4-Results and Discussion

Out-of-plane motion of the ring is considered in the current analysis. Figure 5 shows a comparison between the numerical model (minimum and maximum amplitude), those obtained by finite element analysis (FEA) and through experimental measurement. A frequency sweep is performed in the numerical model and comparisons are made (Figure 5). Reasonable agreement is observed between the numerical predictions and measurements. The first monitored modal response (experimentally obtained) is at 40 Hz with the numerical model closer to the experimental value than that obtained through FEA. The numerical model and FEA predict approximately 185 Hz for the second mode, with the measured equivalent being approximately 100 Hz. The third mode occurs at approximately 400 Hz (experimental), which agrees well with the numerical model and the FEA results.

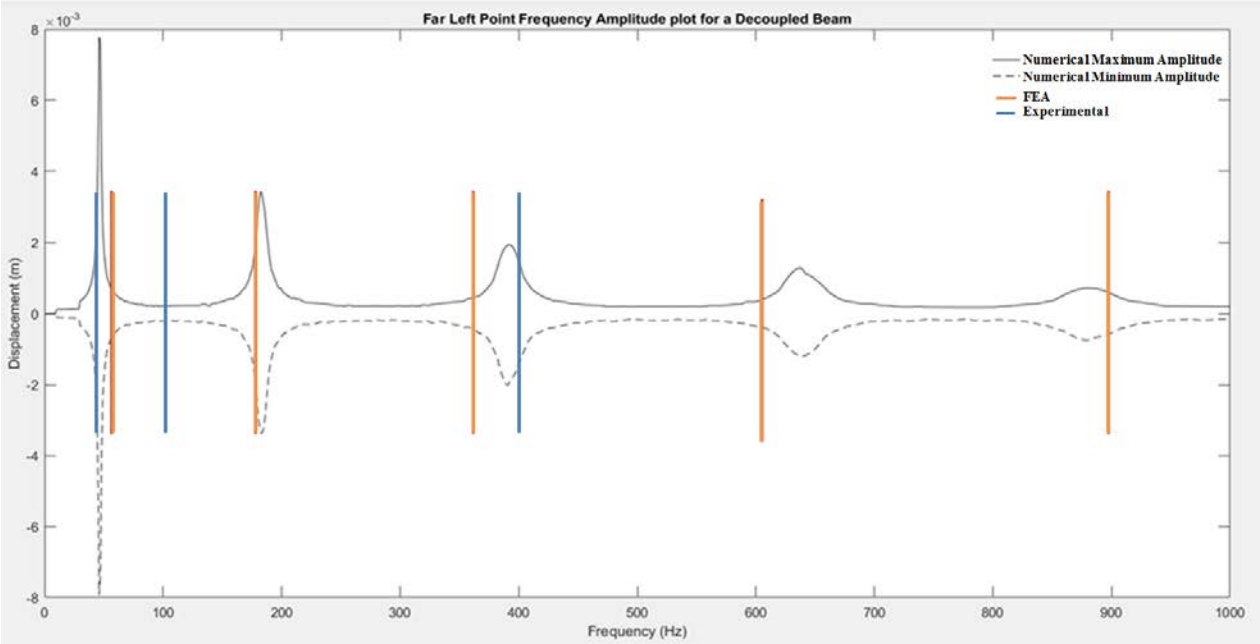

Figure 5: Frequency sweep responses (predictions and measurements)

A frequency sweep is undertaken in the experiments between 10 Hz and 500 Hz to allow the identification of the mode shapes. A conservative time period of 20 seconds is utilised for the frequency sweep in order to ensure the contributions of each mode are fully captured. The frequency amplitude plot from the LDV output is shown in Figure 6. Numerical and FEA results are shown in the amplitude-frequency plot.

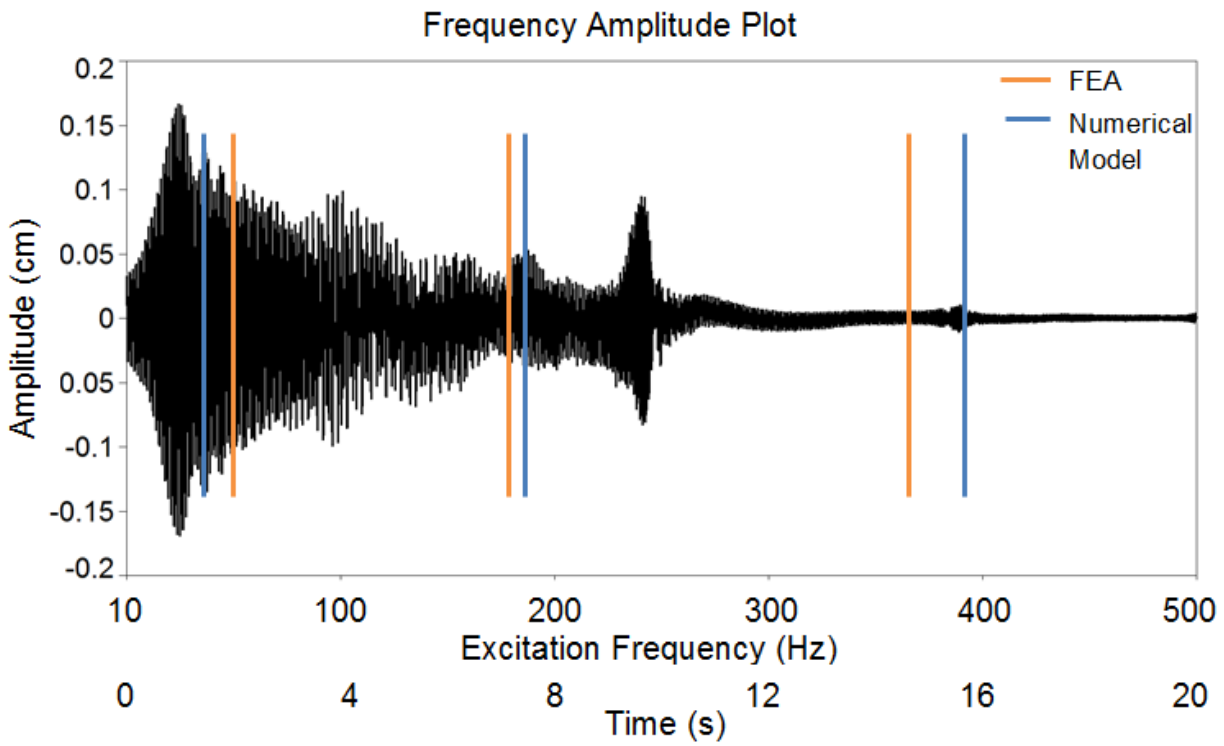

Figure 6: Amplitude-frequency plot (predictions and measurement)

Figure 7 is a continuous wavelet time-frequency (CWT) spectrum of the experimental results of figure 6. Figure 7 (a) depicts the frequency response between 10 Hz and 500 Hz, whereas Figure 7 (b) is that between 300 Hz and 500 Hz, ensuring that the higher frequencies are identified. The current investigation is focused on the out-of-plane motion of the ring. However, in practice the motions are entirely coupled, evident by the presence of the in-plane frequencies in the experimental results. The 250 Hz resonant frequency is caused by the in-plane motion of the ring, demonstrating the effect of coupling. The numerical predictions show close prediction of the frequencies when compared for both the 40 Hz and 480 Hz contributions, with that at 40 Hz being the dominant modal response. Both the numerical and FEA results calculate approximately 180 Hz for the second out-of-plane mode, within an acceptable degree of accuracy with the experimental results.

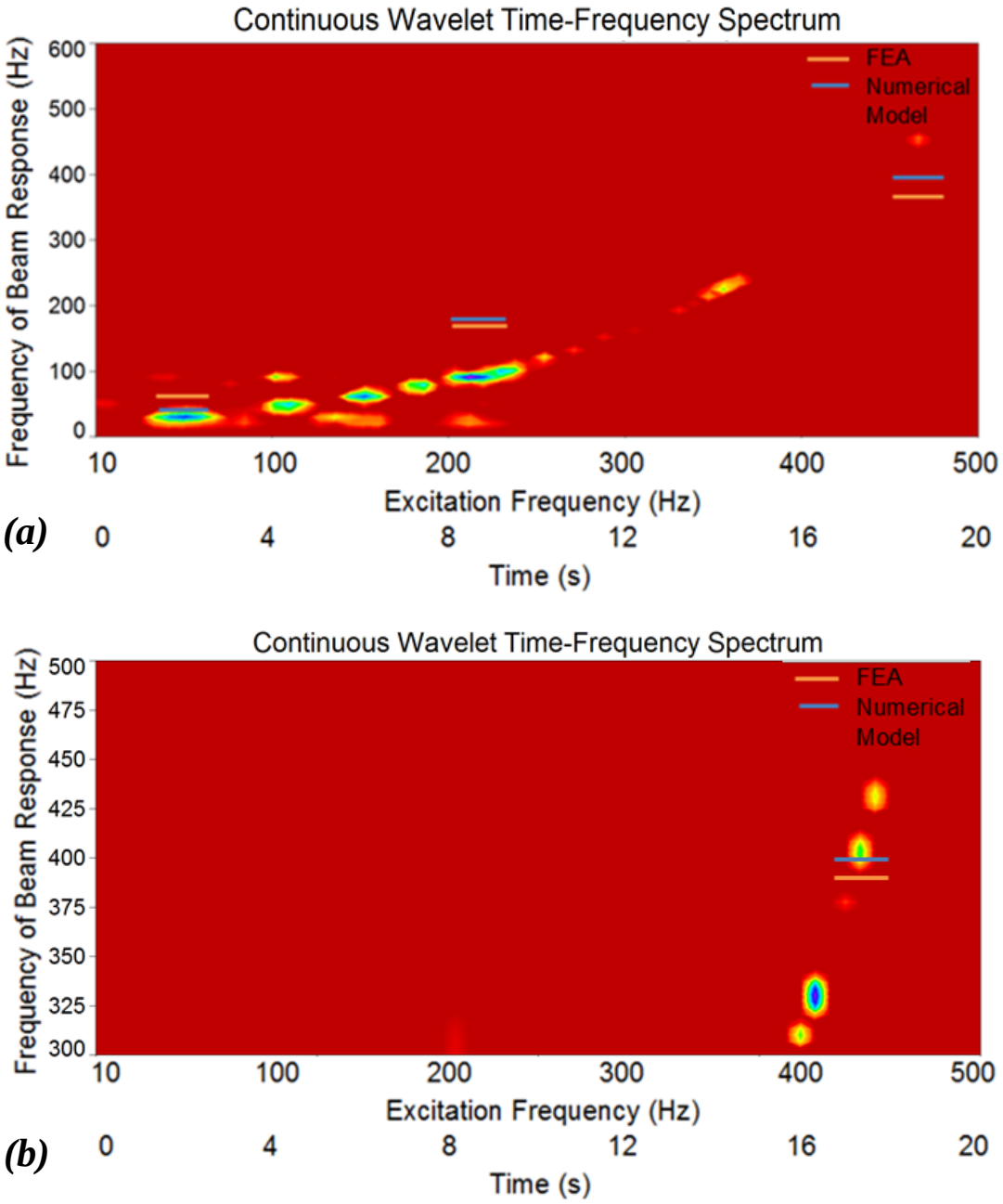

Figure 7. Continuous wavelet spectrum for (a) 10 Hz - 500 Hz and (b) 300 Hz - 500Hz

5- Concluding Remarks

The developed numerical model predicts the modal response of the thin compression ring with good degree of conformance to that obtained using FEA, which requires a much larger computational effort. The results have a reasonably good level of agreement with experimental measurements of the modal response of the ring, mainly for out-of-plane excitation of the ring, close to free-free boundary conditions. The development of the current approach is critical to the

development of a combined tribo-dynamic analysis of the piston ring pack; representing the complex motions of the ring. The study needs to be extended to in situ conditions of the ring within a cylinder, subjected to friction, ring tension and applied variable radial gas and contact pressures. This will constitute the future extension of the current research.

Acknowledgements

The authors would like to express their gratitude to the Engineering and Physical Science Research Council (EPSRC) and AVL List GmbH for the financial support of the reported research under the EPSRC-CDTei collaborative funding.

Nomenclature

A	Cross-sectional area	m^2
b	Thickness of compression ring	m
E	Young's modulus of elasticity	N/m^2
f	Applied vibration frequency	Hz
F_x^i	Force acting on an element in *x* direction for the i^{th} element	N
F_y^i	Force acting on an element in *y* direction for the i^{th} element	N
F_z^i	Force acting on an element in *z* direction for the i^{th} element	N
G	Shear modulus	N/m^2
h	Height of the compression ring	m
J_{yy}	Second area moment of inertia	m^4
J_{zz}	Second area moment of inertia	m^4
J_p	Polar area moment of inertia	m^4
L	Length of the compression ring	m
M	Amplitude of oscillation	m
M_x^i	Moment acting on an element in *x* direction for the i^{th} element	Nm

M_y^i	Moment acting on an element in *y* direction for the ith element	Nm
M_z^i	Moment acting on an element in *z* direction for the ith element	Nm
t	Time	s
v	Poisson's ratio	-
v_f	Excitation velocity	m/s
x, y, z	Cartesian coordinates	-
x_f	Excitation displacement	m
y_α	y component of the shear centre and mass centre coupling arm	m
z_α	z component of the shear centre and mass centre coupling arm	m

Greek Symbols

Δ_x^i	Deflection in *x* for the ith element	m
Δ_y^i	Deflection in *y* for the ith element	m
Δ_z^i	Deflection in *z* for the ith element	m
θ_x^i	Rotation in *x* for the ith element	rad
θ_y^i	Rotation in *y* for the ith element	rad
θ_z^i	Rotation in *z* for the ith element	rad
ρ	Material density	kg/m^3

References:

[1]- Andersson, B.S., "Company's perspective in vehicle tribology", Proc. 18th Leeds-Lyon Symposium, Elsevier Sci., 1991.

[2]- Baker, C.E., Theodossiades, S., Rahnejat, H. and Fitzsimons, B., "Influence of in-plane dynamics of thin compression rings on friction in internal combustion engines", J. Engineering for Gas Turbines and Power, 2012, 134(9):092801.

[3]- Baker, C., Rahmani, R., Theodossiades, S., Rahnejat, H. and Fitzsimons, B., "On the effect of transient in-plane dynamics of the compression ring upon its tribological performance", J. Engineering for Gas Turbines and Power, 2015, 137(3):032512.

[4]- Tian, T., "Dynamic behaviours of piston rings and their practical impact. Part 2: oil transport, friction and wear of ring/liner interface and the effects of piston and ring dynamics", Proc. IMechE, Part J: J. Engineering Tribology, 2002, 216, pp. 229–248.

[5]- Ma, M. T., Smith, E. H., and Sherrington, I., "Analysis of lubrication and friction for a complete piston-ring pack with an improved oil availability model. Part 2: circumferentially variable film", Proc. IMechE, Part J: J. Engineering Tribology, 1997, 211, pp. 17–27

[6]- Akalin, O. and Newaz, G. M., **"**Piston ring cylinder bore friction modelling in mixed lubrication regime. Part I: analytical results", Trans. ASME, J. Tribology, 2001, 123, pp. 211–218.

[7]- Bolander, N. W., Steenwyk, B. D., Sadeghi, F. and Gerber, G. R. "Lubrication regime transitions at the piston ring-cylinder liner interface", Proc. IMechE, Part J: J. Engineering Tribology, 2005, 129, pp. 19–31.

[8]- Mishra, P. C., Balakrishnan, S., and Rahnejat, H., "Tribology of compression ring-to-cylinder contact at reversal", Proc. IMechE, Part J: J. Engineering Tribology, 2008, 222(7), pp. 815–826

[9]- Rahmani, R., Theodossiades, S., Rahnejat, H. and Fitzsimons, B., "Transient elastohydrodynamic lubrication of rough new or worn piston compression ring conjunction with an out-of-round cylinder bore", Proc. IMechE, Part J: J. Engineering Tribology, 2012, 226(4), pp. 284-305

[10]- Morris, N., Rahmani, R., Rahnejat, H., King, P.D. and Fitzsimons, B., "The influence of piston ring geometry and topography on friction", Proc. IMechE, Part J: J. Engineering Tribology. 2012, 227(2), pp. 141-153

[11]- Lang, T. E., "Vibration of Thin Circular Rings - Part 1", Jet Propulsion Laboratory Technical Report, California Institute of Technology, 1962, No.32-26.

[12]- Ojalvo, I.U., "Coupled Twist-Bending Vibrations of Incomplete Elastic Rings", Int. J. Mech. Sci, 1962, 4(1), pp. 53-72.

[13]- Baker, C., Rahnejat, H., Rahmani, R. and Theodossiades, S., "Analytical evaluation of fitted piston compression ring: modal behaviour and frictional assessment", SAE Technical paper, No. 2011-01-1535, 2011

[14]- Baker, C., Rahmani, R., Karagiannis, I., Theodossiades, S., Rahnejat, H. and Frendt, A., "Effect of compression ring elastodynamics behaviour upon blowby and power loss", SAE Technical paper, No. 2014-01-1669, 2014.

[15]- Chidamparam, P. and Leissa, A, W., "Vibrations of planar curved beams, rings, and arches", Applied Mechanics Reviews, 1993, 46(9), pp. 467-483.

[16]- Ejakov, M, A. and Schock, H. J., "Modeling of ring twist for an IC engine", SAE Technical Paper, No. 982693, 1998

[17]- Okamura, H., Shinno, A., Yamanaka, T., Suzuki, A. and Sogabe, K., "Simple modelling and analysis for crankshaft three-dimensional vibrations, part 1: background and application to free vibrations", Journal of vibration and acoustics, 1995, 117(1), pp. 70-79.

[18]- Rahnejat, H., "Multi-body Dynamics: Vehicles, machines and mechanisms", Professional Engineering Publishing, Bury St Edmunds, UK, 1998

[19]- Rao, J. S. and Carnegie, W., "Solution of the equations of motion of coupled-bending bending torsion vibrations of turbine blades by the method of Ritz-Galerkin", Int. J. Mech. Sci., 1970, 12(10), pp. 875-882.

[20]- Timoshenko, S., "Vibration Problems in Engineering", 3rd ed., Van Nostrand, New York, 1955.

[21]- Bell, J. R. and Rothberg, S. J., "Rotational vibration measurements using laser Doppler vibrometry: comprehensive theory and practical application", J. Sound and Vibration, 2000, 238 (4), pp. 673 - 690